Boffin Access

Open Access Journal | Volume: 1.1

Journal of Water technology and Treatment methods

ISSN 2517-7427

Recovery of Phosphate from Mixed Solutions Using Surface Modified Maghemite Nano-Adsorbents

Jonathan A Brant*,
Adam E Marsh

Department of Civil and Architectural Engineering, University of Wyoming, Laramie, USA

Abstract

Waste water is a potentially rich source of valuable materials including nutrients, such as phosphates. Recovering these compounds is difficult because of their relatively dilute concentrations and complex chemistry of the wastewater itself. The purpose of this study was to synthesize super-paramagnetic nanoparticles (maghemite, γ-Fe_2O_3) for recovering phosphate from simple and complex electrolyte solutions. The γ-Fe_2O_3 nanoparticles were coated with dimercaptosuccinic acid (DMSA) onto which a tetraethylenepentamine (TEPA) coating was attached using two different methods. The unmodified and modified nanoparticles were characterized with regards to their size/size distribution, surface charge (zeta potential), surface functionality, and specific surface area, using dynamic light scattering, transmission electron microscopy, laser Doppler velocimetry, Fourier transform infrared spectroscopy, X-ray fluorescence, and BET surface area analysis. The TEPA-functionalized nanoparticles, irrespective of the synthesis method used, achieved phosphate adsorption capacities between 11 to 16 mg PO_4/g adsorbent. Adsorption increased with increasing solution ionic strength up to 100mM NaCl, and decreased with increasing solution pH. Both relationships were attributed to ionic interactions between the phosphate anion and the negatively charged adsorbent surface. The presence of competing anions, nitrate and sulfate, did not significantly affect phosphate adsorption by the TEPA functionalized γ-Fe_2O_3 nanoparticles.

Keywords

Phosphate; Maghemite; Nanoparticle; Resource Recovery; Wastewater

Introduction

In 2005, nearly 150 million tonnes of phosphate rock were extracted for fertilizer production. At current consumption rates, known phosphate reserves are projected to be depleted within 50 to 100 yrs [1]. Increases in phosphate demands are coupled with security concerns associated with the areas in which phosphate deposits are found, such as Morocco. These issues provide strong motivation for developing techniques for recovering phosphate from different wastewaters. Waste waters, including municipal, mine leachate, agricultural runoff, and stock farm collection pits, are all rich in phosphates [2-4]. Phosphate recovery is therefore an attractive proposition if technologically viable.

Existing technologies for removing phosphates from wastewater include crystallization and biological processes [5]. Both of these approaches come with limitations regarding their production of high-purity phosphate. Struvite ($MgNH_4PO_4 \bullet 6H_2O$) formation, a crystallization process, is widely practiced in both municipal and industrial systems [5-6]. Struvite precipitation operates most effectively in solutions with high pH (≥ 7.5), with maximum removal occurring at pH 9, high phosphate concentrations with specific Mg:NH_4:PO_4 molar ratios, and with extended residence times [2]. Because struvite forms through a precipitation process, it will incorporate compounds from the mixture within its crystal structure [2]. These characteristics limit the applicability of this process and the purity of the final product. Biological processes involve condensing dissolved phosphates into a solid state by passing the wastewater through reactors designed to enhance biological uptake of phosphorus by bacteria. Phosphorus accumulating organisms have been reported to contain between 75 and 148 mg P/g biomass [7]. By the nature of biological phosphorus accumulation, the opportunity for beneficial reuse of the bio-solids as fertilizers/soil amendments presents itself. Much of the phosphorus contained in these bio-solids is not in a form that is readily available for plant uptake and must first undergo additional biological degradation after field application. The phosphorus contained within the bio-solids cannot be used for industrial applications because no processes exist to separate phosphorus from the organic constituents [6]. Therefore, techniques that are capable of recovering phosphates under diverse conditions, while producing a high-grade product, are needed.

Previous efforts have focused on developing different types of phosphate adsorbents. Biswas et al., Kuzawa et al., and Ping et al. developed phosphate adsorbents for use in fixed columns made of hydrocalcite, Zn(IV) impregnated orange waste, and La(III)

Article Information

DOI: 10.31021/jwt.20181101
Article Type: Research Article
Journal Type: Open Access
Volume: 1 **Issue:** 1
Manuscript ID: JWT-1-101
Publisher: Boffin Access Limited

Received Date: October 20, 2017
Accepted Date: November 06, 2017
Published Date: January 15, 2018

Citation: Jonathan A Brant, Adam E Marsh (2018) Recovery of Phosphate from Mixed Solutions Using Surface Modified Maghemite Nano-Adsorbents. J Water Technol Treat Methods 1:101

*Corresponding author:

Jonathan A Brant
Department of Civil and Architectural Engineering
University of Wyoming
Laramie, USA
Tel: (307) 766 – 5446
E-mail: jbrant1@uwyo.edu

impregnated zeolite nanoparticles, respectively [8-10]. These materials respectively achieved adsorption capacities of 47, 57, and 25 mg PO_4/g adsorbent. Maximum phosphate adsorption was achieved between pH 2 and 5 for Zn(IV) impregnated orange waste and at pH 4 for La(III) impregnated zeolite nanoparticles. None of the aforementioned studies evaluated the effect of solution ionic strength upon phosphate adsorption, but all attributed adsorption to ion exchange. Given that the adsorption process is ionic in nature it is very likely that solution ionic strength and the presence of competing ions, will negatively affect phosphate adsorption [11-12]. In fact, Biswas et al. and Ping et al. found that competition between Cl^-, HCO_3^-, and SO_4^{2-} with phosphatedid reduce (marginally) adsorption [8,10].

Super-paramagnetic nanoparticles, such as maghemite (γ-Fe_2O_3), are attractive adsorbent materials because of their large specific surface are, customizable surface chemistry and the ability to magnetically separate them from a mixture. γ-Fe_2O_3 nanoparticles are highly paramagnetic with a magnetic saturation between 70 and 76 emu/g for when the diameter is > 25 nm implying a large response to magnetic fields [13-15]. This characteristic is particularly attractive as it affords the possibility of separating the adsorbent/adsorbate complex from solution without the need for clarification or filtration processes [16]. For these reasons they have become the focus of a large body of research on using magnetic nanoparticle for metal recovery from solution [14,17-20]. γ-Fe_2O_3 nanoparticles can adsorb metals in both a bare or surface modified state. Dimercaptosuccinic acid (DMSA) is one surface coating that has been studied because of its stable molecular structure across a wide pH range and ability to prevent particle aggregation at high ionic strengths [21]. Secondary molecules can also be bound to the carboxylates on the DMSA molecule once adsorbed to the γ-Fe_2O_3nanoparticles.Coating Fe_3O_4nanoparticles with DMSA increased copper adsorption in synthetic groundwater and river water from 3.45 mgCu(II)/g to 36.49 mgCu(II)/g and 23.82 mgCu(II)/g, respectively [19,20]. Warner et al. found that DMSA-coated γ-Fe_2O_3nanoparticles having a diameter of 7.2 nm adsorbed 23.8 mg Cu(II)/g compared to 3.5 mg Cu(II)/g for bare γ-Fe_2O_3nanoparticles of equal diameter [19]. Similarly, DMSA-coated γ-Fe_2O_3nanoparticles adsorbed 42.5 mg Pb/g adsorbent while bare γ-Fe_2O_3 nanoparticles adsorbed 6.9 mg Pb/g. The properties of DMSA responsible for increasing adsorption were not investigated in these previous efforts, but are most likely due to increased electrostatic attraction and increased nanoparticle surface area [15,21]. While success has been had with metal adsorption, fewer studies have focused on anions, such as phosphate.

Anion adsorption is more difficult than that for cations, primarily due to their lower charge to mass ratio [22-23]. Because anions are greater in size and mass than cations in general, receptor sites need to be larger and must interact with the anion in more than one location to successfully adsorb it. When an ion adsorbs to a surface, the free energy of the complex must be less than the free energy of the separately solvated partners [24]. Phosphate has a high Gibbs enthalpy of hydration (-2,765 kJ/mol), making its adsorption from solution difficult. In nature, most anion receptors have a flexible structure to more easily accommodate the speciation and orientation of the incoming phosphate ion [24]. Flexible geometry improves adsorption efficiency by expanding the range of conditions under which phosphate adsorption will occur and also enhances adsorbent regeneration. To compensate for this, matching receptor and anion geometry is especially important. Phosphate exists in three major forms – $H_2PO_4^-$, HPO_4^{2-}, and PO_4^{3-} – each being more prevalent within a specific pH range. Optimizing the geometry and charge distribution is important to maximize the free energy reduction that occurs when an anion is adsorbed.

Polyamines are among the most effective and widely used phosphate receptors [11,12]. Amine moieties act as phosphate binders over a wide pH range. When protonated, amine groups can interact electrostatically, with phosphate and act as hydrogen bond sites when interacting with deprotonated phosphate species [22]. When deprotonated, amine groups act as hydrogen bond receptors when interacting with protonated phosphate species. Amines have also been used effectively to remove phosphate through ion exchange [12]. According to Bazzicalupi et al. the two most important considerations for polyamine phosphate binders are the degree of protonation near neutral pH and the spacing of protonated amines [22]. A high degree of protonation near neutral pH maximizes the electrostatic attraction between phosphate and the receptor. Proper spacing enables multiple hydrogen bonds to form simultaneously with a single ion. Polyamines become more ridged as their protonation state increases, to maintain even distribution of positive charges. Xu et al. measured phosphate adsorption capacities for ethylenediamine-triethylamine (EDA-TEA) of approximately 13 mg PO_4/g resin from pH 4 – 9 [12,25]. Saad et al. found that mesoporous silica coated with 3-aminopropyltriethoxsaline (APTES) adsorbed phosphate through electrostatic bonds [11]. The APTES-coated adsorbent achieved a maximum adsorption capacity of 16.5 mg PO_4/g adsorbent at pH 5. Phosphate was bound preferentially over other anions (Cl^-, HCO_3^-, and SO_4^{2-}) with SO_4^{2-} competing most effectively, reducing phosphate adsorption by 42%. Ionic bond formation was found to be exothermic, and accordingly, adsorption proceeded more effectively at lower solution temperatures. Xu et al. found that phosphate adsorption was drastically reduced by increasing solution ionic strength, decreasing nearly 84% from 0 to 0.2 M [12].

The objective of this study was to develop a surface-functionalized super-paramagnetic nanoparticle to selectively recover phosphate from complex mixtures. The physical and chemical properties of the bare and coated nanoparticles were characterized to optimize the coating procedure and for understanding the controlling adsorption mechanism(s). Once developed, the presence of competing ions and solution chemistry (pH, ionic strength) and their effects on adsorption were also studied.

Materials and Methods

Reagents

Maghemite nanoparticles (γ-Fe_2O_3) were coated using dimercaptosuccinic acid (DMSA) and tetraethylenepentamine (TEPA). The DMSA, was acquired from Acros Organics (Fair Lawn, NJ) with a reported purity of ≥ 98%. The DMSA powder was stored in a brown glass container and in a dessicator until used. Technical grade 1-Ethyl-3-(3-dimethylaminopropyl) carbodimide (EDC, Thermo Scientific, Rockford, IL) was used as a cross-linker for the DMSA and the γ-Fe_2O_3 nanoparticles. It was stored in a brown glass container and in a dessicator cabinet. TEPA (Fisher Scientific, Fair Lawn, NJ) was used as the final coating agent for adsorbing phosphate. Sodium chloride was used for adjusting the ionic strength (I_s) of all solutions. Unless otherwise noted all solutions were made using doubly deionized water (DDW) produced from a Millipore Direct-QS purification system. The DDW had an average pH 5.5 and a resistivity of18.2 MΩ-cm at 25°C.

Surface modification of maghemite nanoparticles

Maghemite nanoparticles with purity ≥ 99.5% were purchased from U.S. Research Nanomaterials, Inc. (Houston, TX) and used without further purification. The nanoparticles had reported diameters between 20 nm and 40 nm, which was confirmed through transmission electron microscope (TEM) image analysis of the nanoparticles (Figure 1). γ-Fe_2O_3 nanoparticles are paramagnetic, having a magnetic saturation between 70 and 76 emu/g for nanoparticles with a diameter greater than 25 nm [26]. Below this diameter γ-Fe_2O_3 magnetic saturation declines rapidly, being only 34 emu/g for particles with a diameter of 8 nm [26]. γ- Fe_2O_3 nanoparticles behave this way because, below this diameter, surface effects dominate as the surface area to core volume ration increases [26,27,28]. To ensure that the γ-Fe_2O_3nanoparticles were at, or near, maximum magnetic saturation, a mean diameter between 20 and 40 nm was selected. The γ-Fe_2O_3 nanoparticles were coated with DMSA according to the method developed by Auffan et al [21]. In a 500mL glass jar, 400 mg of γ-Fe_2O_3nanoparticles was dispersed in 400mL of DDW adjusted to pH 2.75 with 6 N hydrochloric acid (purity > 99%). To create a well dispersed γ-Fe_2O_3 nanoparticle suspension, the nanoparticles were sonicated for 30 min at 30% amplitude by

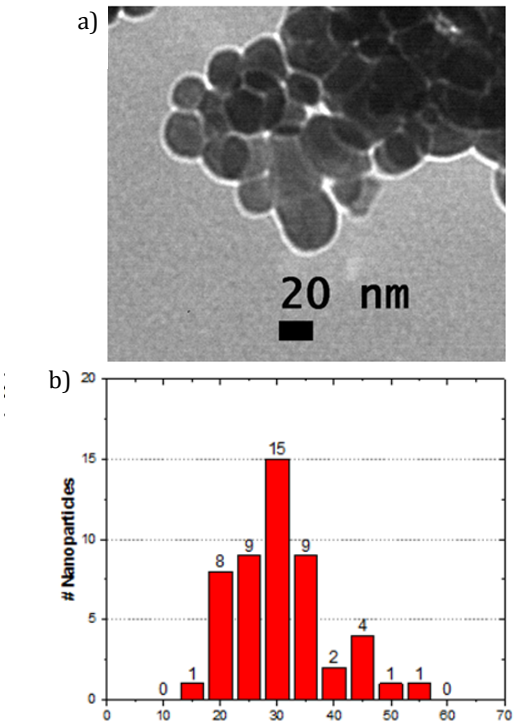

Figure 1: **(a)** Representative TEM image of unmodified γ-Fe_2O_3 nanoparticles. **(b)** Size distribution of γ-Fe_2O_3 nanoparticles based on image analysis of TEM images (n = 50).

a probe sonicator (Fisher Scientific Sonic Dismembrator Model 500, Fair Lawn NJ). Following sonication, the pH of the suspension was verified to be 2.75 and, if needed, adjusted back to this value with 6N hydrochloric acid or 10N sodium hydroxide (purity ≥ 99.5%). Next, the sealed container was bath sonicated for 1 hr (Branson Model 2510, Danbury CT) and then probe sonicated for an additional 30 min at 30% amplitude. Then, 56 mg of DMSA was added to 75mL of DDW in a 100mL glass beaker and the pH was adjusted upwards to 2.75 with 10N sodium hydroxide. The solution was covered and wrapped in tin foil to prevent light exposure. The solution pH was verified after 30mins of mixing and, if needed, was adjusted back to pH 2.75. Once the pH was stable, the solution was covered and constantly mixed. Immediately after sonication, 73.1mLof the DMSA solution was added to the γ-Fe_2O_3nanoparticlesuspensionto create a 6% DMSA: Fe_{total} molar ratio. The DMSA and γ-Fe_2O_3nanoparticlemixturewas transferred to a 1 L glass jar, covered in aluminum foil and placed on an end-over-end mixer for 24 hrs. After mixing, the pH of the DMSA-coated γ-Fe_2O_3suspension was adjusted to pH 11 over the course of 1.5 hrs with 10N sodium hydroxide. This facilitated the replacement of ionic bonds between DMSA's carboxylate groups and γ-Fe_2O_3nanoparticles with covalent bonds between DMSA's thiol groups and the oxygen in the γ-Fe_2O_3nanoparticle lattice structure. The solution was returned to the end-over-end mixer for 2 hrs and then acidified to pH 7 for storage. Equally divided into 250mL plastic bottles, the DMSA-coated γ-Fe_2O_3 nanoparticles were separated from suspension by centrifugation at 22°C for 2 hrs at 16,500 G's.Supernatant was siphoned away as completely as possible without disturbing the particle pellet and then replaced with DDW. DMSA-coated γ-Fe_2O_3nanoparticleswere returned to the 1 L glass jar and placed on the end-over-end mixer for 1 hr. In this way, the DMSA-coated γ-Fe_2O_3 nanoparticles were rinsed 5×with DDW to remove unbound DMSA from solution. The purified DMSA-coated γ-Fe_2O_3 nanoparticles were placed in petri dishes and dried at 45°C. Dehydrated DMSA-coated γ-Fe_2O_3nanoparticles were scraped from the petri dishes and pulverized with a mortar and pestle. The final nanoparticles were placed in a glass vial, capped, wrapped in aluminum foil, and stored under vacuum at 22°C.

Coating Maghemite Nanoparticles with TEPA

Tetraethylenepentamine (TEPA) is a linear polyamide having the chemical structure $H_2N(CH_2)_2NH(CH_2)(CH_2)_2$ $NH(CH_2)_2NH_2$ and was used as a phosphate binder in this study. TEPA contains two primary amines (*pKa* 9.25 and 9.81) and three secondary amines (*pKa* 3.87, 4.92, 8.47). Three of TEPA's five amine moieties are protonated at neutral pH and their positive charges are separate by four ethylene groups; theoretically imparting some flexibility to the molecule. When attached to DMSA the TEPA molecules extend radially outward, presenting prospective phosphate binding sites at two levels. The outermost amine moiety and the middle amine moiety are protonated up to pH 8.5, allowing for the formation of electrostatic and hydrogen bonds over a wide pH range. Because the linear TEPA molecules extend outwards parallel to one another, it is possible that they amine moieties located at the same level on separate molecules can simultaneously bond with a single phosphate molecule [29]. If exposed to alkaline conditions, TEPA can be fully deprotonated, eliminating electrostatic attraction with phosphate ions, opening the possibility that phosphates can be desorbed and recovered. DMSA-coated γ-Fe_2O_3nanoparticles were coated with TEPA EDC. In a 1-step synthesis process, 400 mg of DMSA-coated γ-Fe_2O_3nanoparticles were dispersed in 1 L of DDW with a 0.1 M 3-(N-morpholino) propanesulfonic acid (MOPS) buffer (Thermo Scientific, Rockford, IL). 2.96mM of TEPA was added, the pH was adjusted to 7.1 ± 0.05 using 1.0 M sodium hydroxide and then the solution was sonicated for 10mins. 0.576 g of EDC was dissolved in 57.62mL of DDW to create a 10 mg EDC/mL solution. The EDC solution was added to the nanoparticle suspension and mixed in an end-over-end mixer for 2 hrs. The nanoparticles were rinsed three times with DDW separating the nanoparticles from solution using a LifeSep 50 SX magnet (Dexter Magnetic Technologies, Elk Grove Village, IL). Purified TEPA-coated nanoparticles were then dried at 45°C, pulverized, wrapped in aluminum foil and stored under vacuum at 22°C.

In a 2-step synthesis process, 400 mg of DMSA-coated γ-Fe_2O_3nanoparticles were dispersed in 1 L of DDW with a 0.1 M MOPS buffer and one BupH MES buffered saline pack (Thermo Scientific, Rockford, IL). The buffered DMSA-coated nanoparticle suspension was adjusted to pH 5.8 and 0.663 g of reagent grade Sulfo-NHS (Thermo Scientific, Rockford, IL) and 0.586 g of EDC were added. To activate the EDC crosslinker, the buffered DMSA-nanoparticle suspension was mixed vigorously for 30 min. 0.578 ml of TEPA were dissolved in 29.86mL of DDW and the pH was adjusted to 7.2. After mixing, the buffered DMSA-coated nanoparticle suspension was adjusted to pH 7.2. Combining the TEPA solution and buffered DMSA-coated nanoparticle suspension, the suspension was mixed for 2 hrs. The TEPA-coated nanoparticles were rinsed three times with DDW, separating the nanoparticles from solution using a LifeSep 50 SX magnet. Purified TEPA-coated nanoparticles were then dried at 45°C, pulverized, wrapped in aluminum foil and stored under vacuum at 22°C.

Nanoparticle Surface Chemistry Characterization

Fourier transform infrared spectroscopy (FTIR) measurements were conducted to confirm the surface functionality of bare, DMSA-coated, and TEPA-coated γ-Fe_2O_3nanoparticles. A DMSA sample was also characterized for comparison to the DMSA-coated nanoparticles. FTIR measurements were done using a Perkin-Elmer Spectrum 1000 FTIR Spectrophotometer. Samples were pulverized and combined with a KBr standard (99.3% purity, Fisher Scientific, Fair Lawn, NJ) to produce a homogenous mixture. The sample constituted 1% of the mixture. IR sample cards were prepared by pressing the sample KBr mixture into a semitransparent pellet on a KBr IR card (International Crystal Labs, Garfield, NJ) using a hydraulic press (Wabash MPI, model 50-18-2TM, Wabash, IN). The slide aperture was uniformly covered with approximately 2mm of sample and fused into a pellet with 20,000 lbs of force for 60 secs. IR cards were covered top and bottom with aluminum foil to prevent foreign material from contaminating the sample. The KBr background was measured with 225 sub runs to enhance the noise-to-signal ratio. Samples were measured as a ratio

to the background slide with 225 sub runs. Measured peaks were matched to their corresponding groups using data reported in the literature.

The mass of DMSA that was adsorbed, or bound, to a unit mass of γ-Fe_2O_3 nanoparticles was determined by X-ray fluorescence (PAN anlytical, model X'Pert PRO, Netherlands). The characteristic wavelengths of iron and sulfur emitted by 3 samples were measured and compared to the magnitude of characteristic radiation emitted by standards of known Fe:S concentration. Without further purification, all the samples and standards were measured simultaneously and the S:Fe ratio of the samples was determined from the standard curve generated during the same measurement cycle.

Nanoparticle Size and Surface Charge

Nanoparticle size and zeta potential were characterized using a Malvern ZetaSizer Nano ZS (Malvern Instruments, UK). Average particle size and size distribution were measured as the number weighted hydrodynamic diameter (d_h). To establish consistent nanoparticle concentrations, particles were dispersed in a pre-filtered (0.22 μm) 1mM sodium chloride background electrolyte solution. The solution pH and/or ionic strength (I_s = 1mM sodium chloride for zeta potential measurements) were then adjusted to the desired value using reagent grade hydrochloric acid, sodium hydroxide, and sodium chloride. Approximately 1mL of the nanoparticle suspension was placed in a polystyrene cuvette and sealed with a cap. Size measurements were then taken using a 173°C backscatter angle. All measurements were done at a solution temperature of 25°C, after a 2 min equilibration period, and repeated three times unless otherwise stated. Zeta potential (ζ) was measured by laser Doppler velocimetry to measure the electrophoretic mobility of charged particles moving through an electric field towards an electrode of opposite charge. From this the zeta potential was obtained by applying the Henry equation. Zeta potential measurements used the Smoluchowski approximation of f (Ka) = 1.5 for Henry's equation, as is appropriate for solutions with $I_s \geq$ 1mM [21].

Nanoparticle Surface Area

The specific surface area of bare and DMSA-coated γ-Fe_2O_3 nanoparticles was measured using a TriStar 3000 BET surface area analyzer (Micrometrics Instrument Corporation, Norcross, GA).

Bare nanoparticles were analyzed as supplied by the manufacturer without further preparation. DMSA-coated nanoparticles were dried immediately following synthesis and purification and then pulverized with a ceramic mortar and pestle. Nanoparticle samples and a carbon black standard were placed in sample tubes and degassed overnight at 80°C under a helium atmosphere. Degassed samples were weighed and placed in the analyzer. Analysis was performed using a 5-point Brunauer–Emmett–Teller (BET) isotherm and was checked for accuracy against the simultaneously measured carbon black standard.

Phosphate (PO_4) Adsorption

Phosphate adsorption was evaluated as a function of solution pH and ionic strength. Adsorption was also measured in the presence of sulfate and nitrate. These anions were selected to assess the selectivity of the nanoparticle surface coating for phosphate in waters representative of municipal wastewater. The phosphate stock solution was made to have a phosphate concentration of 2mM. Phosphate adsorption in the presence of sulfate was evaluated using a stock solution having the following composition: 100mM sodium chloride, 2mM phosphate and 2mM sulfate. Similarly, phosphate adsorption in the presence of nitrate was evaluated using a stock solution having the following composition: 2mM phosphate, 2mM nitrate, and 100mM sodium chloride. Stock solutions were synthesized using unbuffered DDW, sodium chloride, sodium phosphate, nitric acid, and sodium sulfate. All solutions were stored in brown glass containers stored at 4°C until used.

Nanoparticle and phosphate concentrations of 5 mg/L and 20 mg/L, respectively were used in those tests where phosphate adsorption was evaluated as a function of solution pH and ionic strength. These concentrations were selected to ensure an excess amount of adsorbate, relative to adsorption sites on the γ-Fe_2O_3 nanoparticles, based on specific adsorption values reported for similar materials [11]. In a brown glass jar, 50mL of DDW was combined with 5 mg of TEPA-DMSA-coated γ-Fe_2O_3 nanoparticles and 0.25mM of a 3-(N-morpholino) propanesulfonic acid buffer to prevent pH drift. The solution was adjusted to the target pH ±0.1 with hydrochloric acid or sodium hydroxide. The TEPA-DMSA-coated γ-Fe_2O_3sodium chloride solution was bath sonicated for 10mins to disperse the sodium chlorides prior to each adsorption test. To 950 ml of DDW was combined with 1.26mL of a 1,583mg/Lphosphate stock solution and sodium chloride was added to achieve the desired experimental I_s. The solution was then mixed in a square reactor at 120 RPMs for 2 hrs. After mixing, a 50mL sample was withdrawn, dispensed into a plastic tube and placed in a LifeSep 50 SX magnetic separator for 10mins to separate the adsorbate-adsorbent complex from solution. A 10mL sample was then withdrawn from the center of the vial and the phosphate concentration measured using a PhosVer 2 reagent (Hach, Loveland, CO). The contents of one PhosVer 2 powder pillow were combined with the 10mL sample and mixed for 15secs. After a 2mins reaction period, the sample absorbance (λ = 711 nm) was measured using a UV-vis spectrophotometer (Shimadzu UV-1800 Spectrophotometer, Japan). The phosphate concentration was calculated from the absorbance using a standard curve.

Adsorption was evaluated in the presence of sulfate and nitrate because these competing ions are ubiquitous in municipal wastewater. In a brown glass jar, 50mL of DDW was combined with 50 mg of TEPA-DMSA-coated γ-Fe_2O_3nanoparticles and the pH was adjusted to 3±0.1 with hydrochloric acid or sodium hydroxide. Next, the TEPA-DMSA-coated γ-Fe_2O_3 nanoparticle solution was bath sonicated for 10mins to ensure nanoparticle dispersion. After 5mins of sonication, solution pH was verified and then returned to the sonicator for an additional 5mins. To evaluate the effect of sulfate competition, 9.7mL of a 100mM sodium chloride and 2mM phosphate stock solutions were added to the nanoparticle/phosphate suspension. To evaluate the effect of nitrate competition, 9.7 ml of a 100mM sodium chloride and 2mM nitrate stock solutions were added to the nanoparticle/phosphate suspension. The complete solution was capped and mixed on an end over end mixer for 2 hrs. 50mL of the solution was placed in a Life Sep 50 SX magnetic separator for 10 min. The phosphate, sulfate and/or nitrate concentrations remaining in solution after adsorbent separation were subsequently measured.

Results and Discussion

Bare and DMSA coated nanoparticle characteristics

Zeta potential as a function of solution pH is reported in Figure 2 for the bare and DMSA-coated γ-Fe_2O_3. The isoelectric point (pH_{iep}) of bare γ-Fe_2O_3 nanoparticles was pH 6.5; the pH_{iep} for the DMSA coated γ-Fe_2O_3s shifted to pH 2.7.Thesevalues agree with previously reported for unmodified (pH_{iep} = 6.3 – 7.8) and DMSA-coated γ-Fe_2O_3 (pH_{iep} < 4) [15,18,30,31]. The shift from pH 6.5 to 2.7 indicates that a DMSA-coating was present on the nanoparticle surface. DMSA's two carboxylate moieties (pKa_1 = 2.7, pKa_2 = 3.5) are responsible for the charge that was measured for the DMSA-coated γ-Fe_2O_3. Because the carboxylate groups on the DMSA molecule protonate as the solution approaches pH 3, the surface charge of DMSA-coated γ-Fe_2O_3 transitioned from negative to positive. The surface charge of DMSA-coated γ-Fe_2O_3 is negative at pH > 3, presenting the possibility for ionic bonds to exist between the nanoparticles and cations. The surface charge for the bare γ-Fe_2O_3 was due to coordination of protons or hydroxyl ions [15].

Specific adsorption capacity (mg adsorbate /g adsorbent) is a function of the available surface area on the adsorbent on which adsorption can occur. It was thus important that the nanoparticles remained in a non-aggregated state during the adsorption process. Aggregation of charged particles is a function of solution pH and I_s) [15,31]. From Figure 3a, the bare γ-Fe_2O_3 nanoparticles aggregated as the solution pH approached the measured pH_{iep} (6.5) for these nanoparticles. Moving away from the pH_{iep} in both directions, the

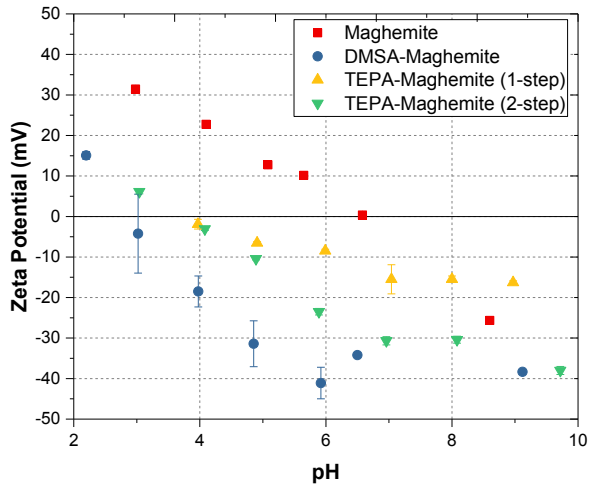

Figure 2: Zeta potential as a function of solution pH for the bare and coated γ-Fe_2O_3 nanoparticles (I_s = 1 mM NaCl, n = 10, T = 25˚C).

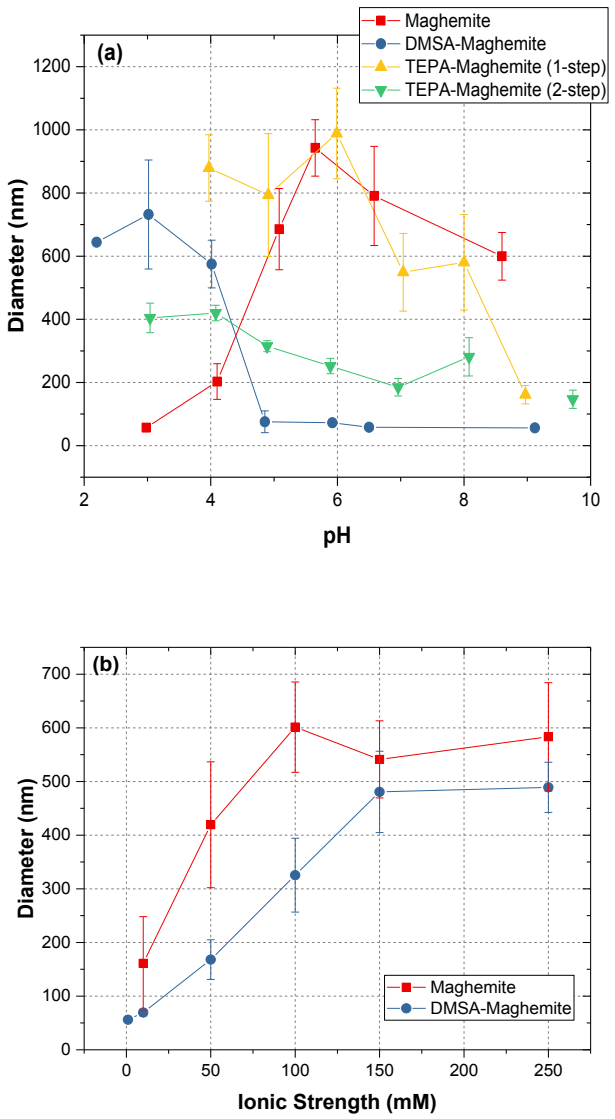

Figure 3: Mean number weighted hydrodynamic diameters of bare and surface modified γ-Fe_2O_3 nanoparticles as a function of (a) solution pH (n = 10, I_s = 1 mM, T = 25°C) and (b) solution ionic strength (n = 3, pH = 9, T = 22˚C).

mean d_h for the bare γ-Fe_2O_3nanoparticles decreased. This supports the idea that the γ-Fe_2O_3 nanoparticleswere stabilized through charge-charge interactions, as repulsive electrostatic interactions become more substantial away from the pH_{iep} for a given surface. Fauconnier et al. found that bare γ-Fe_2O_3nanoparticles, having a pH_{iep} = 7.3, aggregated between pH 5 and 10 in relative agreement with the results presented here [30].

In contrast to the bare γ-Fe_2O_3, the DMSA-coated γ-Fe_2O_3nanoparticles exhibited a consistent d_h of roughly 65 nm at pH ≥ 5 (Figure 3a). The measured pH_{iep} for the DMSA-coated nanoparticles was pH 3.7. Correspondingly, aggregation of the DMSA-coated γ-$Fe_2O_3$was not observed in solutions of pH >5.DMSA-coated γ-Fe_2O_3nanoparticles reached their minimum size (d_h ~ 65 nm) at pH 5 and rapidly aggregated as the pH became more acidic; reaching an apparent maximum size of 730 nm at pH 4. Thus, at pH ≤ 5 the repulsive electrostatic interactions between any two coated nanoparticles were too weak to prevent aggregation. In contrast, bare γ-Fe_2O_3 nanoparticles reached a maximum d_h of 940 nm at pH 5.6 and decreased in size as the solution became more basic or acidic. At pH 3, the unmodified γ-Fe_2O_3nanoparticles were fully dispersed, with a d_h comparable to that of the DMSA-coated γ-Fe_2O_3nanoparticles in solutions of pH ≥ 5. The critical coagulation concentrations (CCC) for the two nanoparticles also differed. The CCC for the unmodified nanoparticles was 50mM, while that for the DMSA coated nanoparticles was 150mM (Figure 3b). This finding further supports our conclusion that the DMSA-coating enhanced the nanoparticle stability through electrosteric interactions.

The specific surface areas (SSA) of bare and DMSA-coated γ-Fe_2O_3nanoparticles were 84.03 ± 0.72 m^2/g and 95.18 ± 0.21 m^2/g, respectively. The SSA measured here compares favorably to the 114 m^2/g measured for 5.8 nm diameter Fe_3O_4- nanoparticles by Yantasee et al. [20]. Thus, the DMSA coating resulted in a 13.3% increase in SSA for the γ-Fe_2O_3. The increase in SSA is attributed to the nanoparticles forming smaller and more fractal aggregate structures. The higher SSA is important because it enabled a greater number of DMSA molecules to be grafted onto the γ-Fe_2O_3. By X-ray fluorescence measurements; DMSA was determined to account for 1.26 ± 0.04% of the coated γ-Fe_2O_3nanoparticles mass. From this, the coating density was determined to be 4.4 × 10^{17} DMSA molecules/m^2. In contrast, the measured SSA of DMSA-coated γ-Fe_2O_3nanoparticles reported here (d_h = 65 nm) far exceeded the theoretical value of 20 m^2/g. This discrepancy between measured and theoretical SSA values indicates that the DMSA-coated γ-Fe_2O_3nanoparticles are likely porous. Again, this is beneficial to the nanoparticle's adsorptive capacity because it provides greater surface area over which adsorption can occur.

Previously, DMSA was reported to form ionic bonds between its thiol groups and the oxygen groups at the surface of γ-Fe_2O_3 [21]. The detection of carboxylic groups and carbon-carbon double bonds at λ = 1620 cm^{-1} and 1410 cm^{-1}, respectively support this structure. No characteristic peaks for thiol groups appeared in the FTIR spectra for the coated γ-Fe_2O_3.This suggests that the thiol groups are located within the interior of the coating and are shielded from detection by carboxylate groups located at the exterior of the coating. Zeta potential measurements also indicated that carboxylate moieties are exposed to the bulk solution because the zeta potential remains constant above pH 8. If thiol groups were present at the outer surface of the coating, their deportation in this range (pKa_1=8.89, pKa_2 = 10.97) would result in a more negative zeta potential. These results agree with the coating structure described by Auffan et al. [14] and Fauconnier et al. [30]

Characteristics and Phosphate Adsorption by γ-Fe_2O_3Nanoparticles Synthesized by the 1-step process

FTIR spectroscopy confirmed that TEPA molecules were grafted to the DMSA-coated γ-Fe_2O_3nanoparticles. Strong adsorption peaks at λ = 2935 and 2808 cm^{-1} corresponded to TEPA's CH_2 bonds and peaks at λ= 3401 and 1664 cm^{-1} corresponded to N-H bonds. This verifies that the coating process successfully bound TEPA molecules to the

DMSA coating. Once bound to DMSA's carboxylate groups, TEPA's primary and secondary amine groups can adsorb phosphate and through electrostatic and hydrogen bonds.

The zeta potential curve of TEPA-coated nanoparticles was distinct from that for the DMSA-coated and bare nanoparticles (Figure 2), by making it more positive. TEPA-coated nanoparticles approached their pH_{iep} at pH 3.97, which was similar to that measured for the DMSA-coated nanoparticles. This was lower than the pH_{iep} reported in the literature for other amine functionalized nanoparticles [32,33]. TEPA molecules possess a net positive charge up to approximately pH 9, where it's final amine moieties deprotonate. If all of the DMSA carboxylate moieties were bound to TEPA molecules, the net nanoparticle surface charge should be positive at pH ~9 [32-34]. Because a portion of DMSA's carboxylate moieties remained unbound to TEPA molecules; the coating process could be further optimized to achieve greater TEPA functionalization.

The d_h of the TEPA-coated nanoparticles made with the 1-step coating process was much greater than DMSA-coated γ-Fe_2O_3 across the measured pH range (Figure 3a). Because the magnitude of the zeta potential for the TEPA-coated nanoparticles was relatively low ($\zeta \leq$), repulsive electrostatic forces were insufficient to prevent aggregation. Only at pH 9 (ζ = -16.5 mV) did the d_h of the TEPA-coated nanoparticles approach that of the DMSA-coated nanoparticles (Figure 3b). The observed decrease in size from pH 6 to 9 did not correlate with an increase in surface charge (i.e., the zeta potential did not change considerably after pH 7), indicating that steric repulsion may contribute to stability. Three of TEPA's five amine groups deprotonate in this range (pKa_3 = 8.47, pKa_4 = 9.25, pKa_5 = 9.81) and, even though the deportation of these groups is not reflected in the zeta potential values, the presence of uncharged molecules on the nanoparticle surface would greatly aid steric stabilization. Being in an aggregated greatly reduces the nanoparticle SSA and is likely to reduce phosphate adsorption capacity. If the magnitude of the zeta potential was increased, the d_h may have decreased further as increasing electrostatic repulsion further stabilizes the nanoparticles. The large d_h of the TEPA-coated nanoparticles may have also been due to TEPA bridges forming between DMSA-coated nanoparticles during the synthesis process. Because TEPA possesses a primary amine at both ends of the molecule, it is possible that separate nanoparticles were bound to both ends of some TEPA molecules. A series of these bridges could explain why the minimum measured d_h of the TEPA-coated nanoparticles was 3× that of the DMSA-coated nanoparticles (Figure 4).

Phosphate adsorption capacity of the TEPA-DMSA-coated γ-Fe_2O_3 nanoparticles, made using the 1-step process was evaluated as a function of solution pH, I_s, and in the presence of competing ions. Phosphate adsorption decreased with increasing solution pH (I_s = 10mM NaCl) from 12 mg PO_4/g nanoparticles at pH 3 to 3.6 mg PO_4/g nanoparticles at pH 6 (Figure 5). Phosphate adsorption measured here is comparable to the 10.7 mg PO_4/g amine functionalized sawdust reported by Unnithan et al. [35], but lower than the 34 mg PO_4/g MCM-48–NH_3^+ reported by Saad et al [11]. Increased phosphate adsorption in more acidic solutions was likely due to the more positive zeta potential of the TEPA-DMSA-coated nanoparticles. Between pH 3 and 6, phosphate is primarily in the form $H_2PO_4^-$ (pK_{a1} = 2.14, pK_{a2} = 7.20) causing phosphate and the negative sites on the nanoparticles to be electrostatically repulsive. To approach local, positively charged TEPA molecules, phosphate must first overcome the net negative charge on the nanoparticle surface. Because of this, as the zeta potential of TEPA-coated nanoparticles becomes less negative, electrostatic bonds between the phosphate and the greater number of positively charged sites on the nanoparticle was formed more easily. Hydrogen bonds between polar phosphate and polar deprotonated amine groups also occur more easily as the net surface charge becomes less negative [35]. Improving the synthesis process so that TEPA molecules are bound to a greater percentage of the carboxylate moieties is likely to improve phosphate adsorption. Acidifying the solution may also aid phosphate adsorption by decreasing competition from hydroxyl anions for adsorption sites

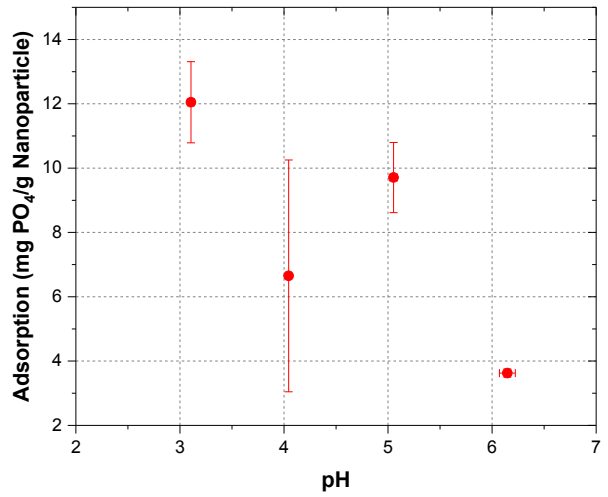

Figure 4: Phosphate adsorption as a function of solution pH by the TEPA-DMSA γ-Fe_2O_3 nanoparticles synthesized using the 1-step process ($n \geq 3$, I_s = 10 mM, T = 25°C). Error bars are shown for both solution pH and phosphate adsorption.

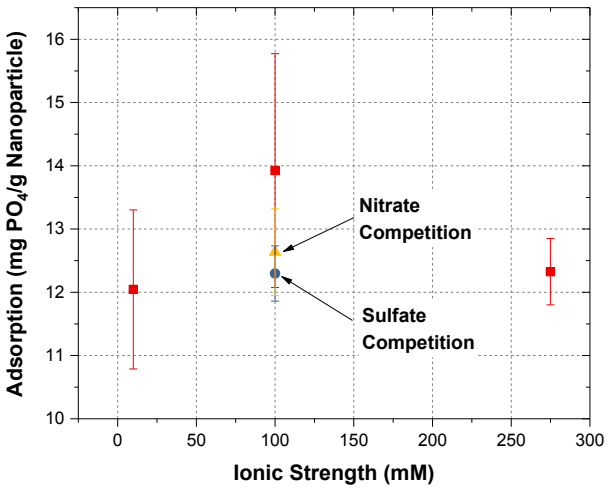

Figure 5: Phosphate adsorption statistics for the TEPA-DMSA-coated γ-Fe_2O_3 nanoparticles synthesized using the 1-step process as a function of solution ionic strength and in the presence and absence of sulfate and nitrate (n = 3, pH = 3, T = 25°C, [PO_4] = 0.33 mM, [SO_{42-}] = 0.33 mM).

[11]. Because phosphate adsorbs to TEPA's primary and secondary amine groups by ionic and hydrogen bonds, increasing solution pH is likely to induce desorption. This presents the opportunity to regenerate the nanoparticles by alkalinizing the solution to near neutral pH.

Phosphate adsorption improved from 9.5 ± 0.2 to 13.9 ± 1.8 mg PO_4/g nanoparticleas I_s increased from 10 to 100mM (Figure 6). This agrees with the hypothesis that phosphate ions must overcome the net negative zeta potential of the TEPA-DMSA-coated nanoparticles before interacting with positively charged amine groups. Increasing I_s compresses the electrostatic double layer, reducing the energy required to overcome like-charge repulsion and enabling phosphate ions to interact more easily with positively charged TEPA amine groups [22,36]. Adsorption decreased at $I_s \geq$100mM due to increased competition between the phosphate and chloride ions and decreasing ion activity Saad et al. reported that increasing the I_s to 2.8mM sodium chloride at pH 4 decreased phosphate adsorption by 9.7% Unnithan et al reported that increasing the I_s from 0 to 1mM sodium chloride decreased phosphate adsorption by approximately 4% [11,35,37]. In

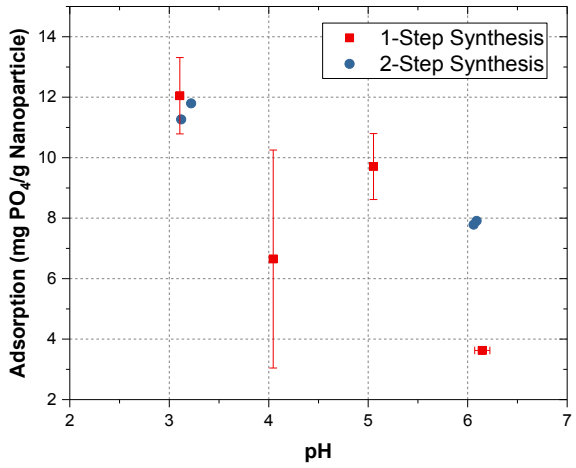

Figure 6: Phosphate adsorption as a function of solution pH by TEPA-DMSA-coated γ-Fe2O3 nanoparticles synthesized by the one and two-step synthesis procedures ($n \geq 2$, I_s = 10 mM, T = 25°C).

comparison, phosphate adsorption was independent of increasing I_s from 10 to 250mM sodium chloride.

Phosphate adsorption was 12.3 and 12.6mg PO_4/g nanoparticle, respectively, in the presence of sulfate and nitrate (Figure 5). This is in comparison to 13.9 mg PO_4/g nanoparticle when only phosphate was present. This translated to an 11.5% and 9.3% decrease in adsorption, respectively, when sulfate or nitrate were present. This adsorption characteristic is highly desirable because sulfate and nitrate are common in municipal and agricultural wastewaters. The effect of sulfate and nitrate ions measured here is comparable to the findings of Unnithan et al. who found that phosphate adsorption by Fe(III)-loaded carboxylated polyacrylamide-grafted sawdust decreased by 9% and 7%, respectively in the presence of 0.5mM sulfate and nitrate [35].

Characteristics and Phosphate Adsorption by γ-Fe_2O_3Nanoparticles Synthesized by a 2-step Process

To maximize phosphate adsorption, it is necessary to create positively charged nanoparticles so that the negatively charged phosphate ion is drawn to the adsorbent. In an attempt to achieve this, a second synthesis process was employed to improve the adsorption of the TEPA to the DMSA coated nanoparticle surface. This was done using Sulfino-NHS to increase the half-life of activated carboxylate groups on the DMSA molecule. A longer half-life extends the period over which TEPA can successfully bind to a given carboxylate group. In this way, the functionalization of carboxylate groups with TEPA may occur more efficiently, resulting in fewer unbound carboxylate groups and a more positive surface charge. This would aid adsorption by allowing phosphate to approach nanoparticles more easily and providing more adsorption sites (primary and secondary amines).

The pH_{iep} for the TEPA-DMSA-coated γ-Fe_2O_3 nanoparticles synthesized with the 2-step process was pH 3.7 (Figure 2), which was one pH unit higher than that for the DMSA-coated nanoparticles and similar to that of the TEPA-DMSA-coated γ-Fe_2O_3 nanoparticles made with the 1-step process. From pH 4 to 7 DMSA's carboxylate groups and TEPA's first 2 amine groups deprotonate, causing the zeta potential to become more negative. Above pH 8, the zeta potential decreased again as TEPA's final 3 amine groups deprotonated. Above the pH_{iep}, the zeta potential of the 1- and 2-step synthesized TEPA-coated nanoparticles diverged. Those nanoparticles made with the 2-step process had a zeta potential that was twice that of its counterpart from pH 5 to 8 (Figure 2). Based on the zeta potential results it was assumed that those nanoparticles made with the 1-step process were more thoroughly coated with TEPA. As more of DMSA's carboxylate groups were functionalized with TEPA, the zeta potential should become less negative. If all carboxylate groups were functionalized with TEPA molecules, the nanoparticles would be positively charged up to pH 9, where TEPA's final amine group deprotonated. The more negative zeta potential that was measured for the TEPA-coated nanoparticles synthesized by the 2-step process indicated a greater number of unbound carboxylate groups on the nanoparticle surface.

In agreement with the more negative zeta potential, the nanoparticles synthesized with the 2-step process were better dispersed over the studied pH range (Figure 3a). These nanoparticles reached a minimum size (d_h = 147 nm) at pH 9.7, and a maximum size (d_h = 400 nm) at their pH_{iep}. The maximum d_h that was measured for the nanoparticles synthesized using the 2-step process was smaller than that for both the bare and DMSA-coated nanoparticles despite having a zeta potential value of lower magnitude than the DMSA-coated nanoparticles (Figure 2). This would suggest that the adsorbed TEPA molecules were enhancing the stability of the nanoparticles in some manner, likely through electrosteric interactions.

The adsorption characteristics of the 2-step TEPA-DMSA-coated nanoparticles was evaluated at pH 3 and 6 and compared to the performance of 1-step TEPA-DMSA-coated nanoparticles (Figure 5). At pH 3, where both particles possess a slight net positive charge, 1- and 2-step TEPA-DMSA-coated nanoparticles performed equally. At pH 6, the TEPA-coated nanoparticles made with the 2-step coating process adsorbed twice as much phosphate as did those prepared with the 1-step process. This was surprising given that the zeta potential of the nanoparticles made with the 2-step process was -24 mV compared to -8 mV for those made with the 1-step coating process. This runs counter to the theory that adsorption decreases as the surface charge becomes more negative, creating greater difficulty for phosphate to approach and adsorb to local positive adsorption sites. The smaller d_h that was measured for the nanoparticles made with the 2-step process was likely the cause of this difference in adsorption. At pH 3, where conditions are most favorable to phosphate adsorption, the smaller diameter of the 2-step TEPA-DMSA-coated nanoparticles provided a sufficiently higher surface area to overcome the less favorable charge conditions for adsorption. At pH 6, the 1-step TEPA-coated nanoparticles reached their greatest average d_h, while the d_h of the 2-step TEPA-coated nanoparticles hydrodynamic diameter decreased 38%. Increased surface area may offset less favorable adsorption conditions at pH 6 effectively enough that, despite having a more negative zeta potential, 2-step TEPA-nanoparticles maintain their adsorptive capacity more effectively than 1-step TEPA-nanoparticles. This underscores the importance of nanoparticle size to a material's adsorption capacity.

Conclusion

Procedures were successfully develop for coating γ-Fe_2O_3 nanoparticles with DMSA and TEPA surface coatings with the goal of adsorbing phosphates from complex mixtures. The coatings both enhanced the stability of the γ-Fe_2O_3 nanoparticles over extended pH and I_s conditions, which was due to electrosteric interactions. A maximum specific phosphate adsorption capacity of 12 mg PO_4/g nanoparticle was measured at pH 3 for both the 1- and 2-step synthesis procedures. Adsorption capacity decreased with increasing pH due to the development of repulsive electrostatic interactions between the coated NP surface and the deprotonated phosphate species. Increasing solution I_s from 10 to 50mM increased phosphate adsorption to an average of 13.9 mg PO_4/g nanoparticle. Further increasing the I_s to 275mM did affect the adsorption capacity. The presence of competing ions sulfate and nitrate at an equal molar ratio to phosphate was found to decrease average phosphate adsorption to 12.3 and 12.6 mg PO_4/g nanoparticle, respectively (I_s=100mM).

References

1. Cordell D, White S (2011) Peak Phosphorus: Clarifying the Key Issues of a Vigorous Debate about Long-Term Phosphorus Security. Sustainability 3: 2027-2049. doi: 10.3390/su3102027

2. Hutnik N, Wierzbowska B, Matynia A (2013) Continuous reactive crystallization of struvite from a solution containing phosphate (V) and potassium ions. Braz J Chem Eng 33: 791-795. doi:10.1590/0104-6632.20160332s00003385
3. Lu SY, Wu FC, Lu Y, Xiang CS, Zhang PY, Jin CX (2009) Phosphorus removal from agricultural runoff by constructed wetland. Ecol Eng 35: 402-409. doi: 10.1016/j.ecoleng.2008.10.002
4. Johns M R (1995) Developments in wastewater treatment in the meat processing industry: A review. Bio resource Technol 54: 203-216. doi: 10.1016/0960-8524(95)00140-9
5. Morse GK, Brett SW, Guy JA, Lester JN (1998) Review: Phosphorus removal and recovery technologies. Sci Total Environ 212: 69-81. doi: 10.1016/S0048-9697(97)00332-X
6. De Bashan LE, Bashan Y (2004) Recent advances in removing phosphorus from wastewater and its future use as fertilizer (1997-2003). Water Res 38: 4222-4246. doi: 10.1016/j.watres.2004.07.014
7. Li N, Ren NQ, Wang XH, Kang H (2010) Effect of temperature on intracellular phosphorus absorption and extra-cellular phosphorus removal in EBPR process. Bioresource Technol 101: 6265-6268. doi: 10.1016/j.biortech.2010.03.008
8. Biswas BK, Inoue K, Ghimire KN, Harada H, Ohto K, et al. (2008) Removal and recovery of phosphorus from water by means of adsorption onto orange waste gel loaded with zirconium. Bioresource Technol 99: 8685-8690. doi: 10.1016/j.biortech.2008.04.015
9. Kuzawa K, Jung YJ, Kiso Y, Yamada T, Nagai M, et al. (2006) Phosphate removal and recovery with a synthetic hydrotalcite as an adsorbent. Chemosphere 62: 45-52. doi: 10.1016/j.chemosphere.2005.04.015
10. Ping N, Bart HJ, Bing L, Lu XW, Zhang (2008) Phosphate removal from wastewater by model-La(III) zeolite adsorbents. J Environ Sci-China 20: 670-674. doi: 10.1016/S1001-0742(08)62111-7
11. Saad R, Belkacemi K, Hamoudi S (2007) Adsorption of phosphate and nitrate anions on ammonium-functionalized MCM-48: Effects of experimental conditions. J Colloid Interf Sci 311: 375-381. doi: 10.1016/j.jcis.2007.03.025
12. Xu X, Gao BY, Tan X, Yue QY, Zhong QQ, et al (2011) Characteristics of amine-crosslinked wheat straw and its adsorption mechanisms for phosphate and chromium (VI) removal from aqueous solution. Carbohyd Polym 84:1054-1060. doi: 10.1016/j.carbpol.2010.12.069
13. Asuha S, Zhao YM, Zhao S, Deligeer W (2012) Synthesis of mesoporous maghemite with high surface area and its adsorptive properties. Solid State Sci 14: 833-839. doi: 10.1016/j.solidstatesciences.2012.04.011
14. Auffan M, Rose J, Proux O, Borschneck D, Masion A, et al. (2008) Enhanced adsorption of arsenic onto maghemites nanoparticles: As(III) as a probe of the surface structure and heterogeneity. Langmuir 24: 3215-3222. doi: 10.1021/la702998x
15. Fauconnier N, Pons JN, Roger J, Bee A (1997) Thiolation of maghemite nanoparticles by dimercaptosuccinic acid. J Colloid Interf Sci 194: 427-433. doi: 10.1006/jcis.1997.5125
16. Berkowit HD, Miller LD, Itskovit Hd (1969) The Influence of Renin-Angiotensin System on Renal Function - Possible Role in Advanced Liver Disease. Brit J Surg 56: 623
17. Chowdhury SR, Yanful EK (2010) Arsenic and chromium removal by mixed magnetite-maghemite nanoparticles and the effect of phosphate on removal. J Environ Manage 91: 2238-2247. doi: 10.1016/j.jenvman.2010.06.003
18. Hu J, Chen GH, Lo IMC (2005) Removal and recovery of Cr (VI) from wastewater by maghemite nanoparticles. Water Res 39: 4528-4536. doi: 10.1016/j.watres.2005.05.051
19. Warner CL, Addleman RS, Cinson AD, Droubay TC, Engelhard MH, et al. (2010) High-Performance, Superparamagnetic, Nanoparticle-Based Heavy Metal Sorbents for Removal of Contaminants from Natural Waters. Chemsuschem 3: 749-757. doi: 10.1002/cssc.201000027
20. Yantasee W, Warner CL, Sangvanich T, Addleman RS, Carter TG, et al. (2007) Removal of heavy metals from aqueous systems with thiol functionalized superparamagnetic nanoparticles. Environ Sci Technol 41: 5114-5119. doi: 10.1021/es0705238
21. Auffan M, Decome L, Rose J, Orsiere T, De Meo M, et al. (2006) In vitro interactions between DMSA-coated maghemite nanoparticles and human fibroblasts: A physicochemical and cyto-genotoxical study. Environ Sci Technol 40: 4367-4373. doi: 10.1021/es060691k
22. Bazzicalupi C, Bencini A, Lippolis V (2010) Tailoring cyclic polyamines for inorganic/organic phosphate binding (vol 39, pg 3709, 2010). Chem Soc Rev 39 (12), 5069-5069.
23. Beer PD, Gale PA (2001) Anion recognition and sensing: The state of the art and future perspectives. Angew Chem Int Edit 40: 486-516. doi: 10.1002/1521-3773(20010202)40:3<486::AID-ANIE486>3.0.CO;2-P
24. Schmidtchen FP, Berger M (1997) Artificial organic host molecules for anions. Chem Rev 97: 1609-1646. doi: 10.1021/cr9603845
25. Xu X, Gao BY, Yue QY, Zhong QQ, Li QA (2011) Preparation of new types of anion exchange resins from agricultural by-products and their utilization in the removal of various toxic anions from solutions. Chem Eng J 167: 104-111. doi: 10.1016/j.cej.2010.12.008
26. Berkowitz A, Schuele W, Flanders P (1969) Influence of crystallite size on the magnetic properties of acicular γ-Fe2O3 particles. Journal of Applied Physics 39: 1261-1263. doi: 10.1063/1.1656256
27. Coey JMD (1971) Noncollinear Spin Arrangement in Ultrafine Ferrimagnetic Crystallites. Phys Rev Lett 27: 1140. doi: 10.1103/PhysRevLett.27.1140
28. Thapa D, Palkar V, Kurup M, Malik S (1994) Properties of magnetite nanoparticles synthesized through a novel chemical route; Cornell University Library: Online
29. Ozmen M, Can K, Arslan G, Tor A, Cengeloglu Y, et al. (2010) Adsorption of Cu(II) from aqueous solution by using modified Fe3O4 magnetic nanoparticles. Desalination 254: 162-169. doi: 10.1016/j.desal.2009.11.043
30. Fauconnier N, Bee A, Roger J, Pons JN (1999) Synthesis of aqueous magnetic liquids by surface complexation of maghemite nanoparticles. J Mol Liq 83: 233-242. doi: 10.1016/S0167-7322(99)00088-4
31. Liu YX, Chen ZP, Gu N, Wang JK (2011) Effects of DMSA-coated Fe3O4 magnetic nanoparticles on global gene expression of mouse macrophage RAW264.7 cells. Toxicol Lett 205: 130-139. doi: 10.1016/j.toxlet.2011.05.1031
32. Jana NR, Earhart C, Ying JY (2007) Synthesis of water-soluble and functionalized nanoparticles by silica coating. Chem Mater 19: 5074-5082. doi: 10.1021/cm071368z
33. Mikhaylova M, Kim DK, Berry CC, Zagorodni A, Toprak M, et al. (2004) BSA immobilization on amine-functionalized superparamagnetic iron oxide nanoparticles. Chem Mater 16: 2344-2354. doi: 10.1021/cm0348904
34. Butterworth MD, Corradi R, Johal J, Lascelles SF, Maeda S, et al. (1995) Zeta-Potential Measurements on Conducting Polymer-Inorganic Oxide Nanocomposite Particles. J Colloid Interf Sci 174: 510-517. doi: 10.1006/jcis.1995.1418
35. Unnithan MR, Vinod VP, Anirudhan TS (2002) Ability of iron(III)-loaded carboxylated polyacrylamide-grafted sawdust to remove phosphate ions from aqueous solution and fertilizer industry wastewater: Adsorption kinetics and isotherm studies. J Appl Polym Sci 84: 2541-2553. doi: 10.1002/app.10579

36. Ditsch A, Laibinis PE, Wang DIC, Hatton TA (2005) Controlled clustering and enhanced stability of polymer-coated magnetic nanoparticles. Langmuir 21: 6006-6018. doi: 10.1021/la047057+

37. Das N (2010) Recovery of precious metals through biosorption - A review. Hydrometallurgy 103: 180-189. doi:10.1016/j.hydromet.2010.03.016